Meteoritics & Planetary Science 37, 1541–1553 (2002)
Available online at http://www.uark.edu/meteor

Experimental approach to generate shock veins in single crystal olivine by shear melting

FALKO LANGENHORST[1]*, JEAN-PAUL POIRIER[1], ALEXANDER DEUTSCH[2] AND ULRICH HORNEMANN[3]

[1]Bayerisches Geoinstitut, Universität Bayreuth, D-95440 Bayreuth, Germany
[2]Institut für Planetologie, Universität Münster, Wilhelm-Klemm-Strasse 10, D-48149 Münster, Germany
[3]Ernst-Mach-Institut, Fraunhofer-Institut für Kurzzeitdynamik, Am Klingelberg 1, D-79588 Efringen-Kirchen, Germany
*Correspondence author's e-mail address: Falko.Langenhorst@uni-bayreuth.de

(Received 2002 April 16; accepted in revised form 2002 July 22)

Abstract–A shock experiment has been devised to produce large shear in a single crystal sample of olivine. The recovered sample exhibits macroscopic shear faults resembling shock veins in ordinary chondrites. Examination with transmission electron microscopy reveals a high density of dislocations in the bulk olivine. The shear faults appear as thin veins containing small grains of olivine and pockets of glass. The microstructure and composition of the material in the veins point to fractional crystallization of a melt. An order of magnitude calculation is consistent with the idea that the veins were produced by shear melting. These results support the view that shock veins in meteorites are the result of shear heating rather than of pressure heterogeneities.

INTRODUCTION

Heavily shocked meteorites are the almost only accessible rocks containing pristine high-pressure silicates (*e.g.*, ringwoodite, wadsleyite, akimotoite, *etc.*) that otherwise are expected to occur in the Earth's transition zone and lower mantle (Madon and Poirier, 1983; Price *et al.*, 1983; Chen *et al.*, 1996; Langenhorst and Poirier, 2000a,b). The high-pressure phases are concentrated in thin black veins, so-called shock veins, which irregularly transect the bulk meteorite. To understand the origin of these high-pressure phases, one has basically to know how the veins form and evolve during shock compression and decompression. Observations on meteorites show that shock veins represent localized melt zones, which due to the presence of high-pressure minerals must have been quenched during shock compression and/or decompression (Stöffler *et al.*, 1991; Langenhorst *et al.*, 1995). Recent theoretical calculations support this view and demonstrate that the time for crystallization of a melt vein is distinctly shorter than the shock duration (Langenhorst and Poirier, 2000b). The veins penetrate not only along grain boundaries but also cut through minerals. Shear mechanisms and/or pressure heterogeneities resulting from density gradients are discussed as potential heat sources for localized melting.

To simulate frictional melting, welding apparatus have been used (Spray, 1987; van der Bogert *et al.*, 2000), but there have been only few experimental attempts to approach this problem with shock techniques. In a previous experimental study (Kenkmann *et al.*, 2000), the role of lithological interfaces has been examined. Here, we focus on the formation of veins within a single mineral.

According to one theory, it is assumed that pressure excursions and hence temperature extremes play an important role in the formation of melt veins in meteorites (Stöffler *et al.*, 1988, 1991). However, there is no physical reason why pressure heterogeneities should be distributed along irregular veins. Instead, offsets along veins demonstrate that shearing is involved in the formation of the shock veins, and that shear heating might be the cause of melting. Therefore, with the view to assess the importance of shear heating, we performed a shock experiment on single crystal olivine, the most abundant mineral in chondritic meteorites, with a special design that maximizes the shearing of the specimen. The use of a single crystal was aimed to avoid pressure heterogeneities and to test whether shearing alone would cause localized melting.

EXPERIMENTAL TECHNIQUES

High-Explosive Shock Experiment

The sample material was a high-quality single crystal olivine from San Carlos (89 mol% forsterite); its composition is given in Table 1. A 3 mm thick, 10 mm diameter disc with well-polished, plane parallel faces was machined out of this single crystal.

The shock experiment was performed using a conventional high-explosive setup, with the specimen encapsulated in a pure (Armco) iron container (Hornemann and Müller, 1971;

Prelude preprint MS#4812

TABLE 1. Representative chemical compositions of host olivine as well as of the core and rim regions of newly formed olivine and interstitial glass in shear faults.

wt%	Host olivine	Olivine core	Olivine rim	Interstitial glass
Si	18.9	19.6	18.1	15.6
Fe	8.1	4.5	15.9	40.8
Mg	29.3	31.4	24.1	7.4
Ca	0.1	n.d.	0.4	0.9
Mn	0.1	0.1	0.2	0.4
Ni	0.2	0.2	0.2	0.2
O	43.3	44.3	41.2	34.8
Number of cations				
Si	1.00	1.01	1.00	1.02
Fe	0.21	0.12	0.44	1.34
Mg	1.78	1.87	1.54	0.56
Ca	<0.01	n.d.	0.02	0.04
Mn	<0.01	<0.01	0.01	0.01
Ni	0.01	<0.01	<0.01	0.01
Σ Cations	3.00	2.99	3.00	2.98
Fo (mol%)	89.3	94.1	77.7	29.4

n.d. = not detected.

Langenhorst and Deutsch, 1994). In this type of experiments, the ignition of the high-explosive (Octogen) causes the acceleration of a thin iron flyer plate. The shock wave is generated by the impact of the flyer plate against the container. To avoid destruction of the container, it was embedded into a steel block that acted as a momentum trap. As an important modification to previous designs, a cylindrical, 6 mm diameter hole was drilled below the specimen disc along the central axis of the container (Fig. 1; see also Ivanov *et al.*, 2002). There was thus a significant portion of free surface at the rear side of the olivine crystal. This modification was introduced to allow the material to flow behind the shock front into the empty cavity, leading consequently to intense deformation and shearing of the olivine specimen.

The shock pressure generated in the iron container was measured in separate calibration experiments. We used the so-called "pin-contact" technique (Müller and Hornemann, 1969; Langenhorst *et al.*, 2002) to measure the free-surface velocity (twice the particle velocity) at the rear side of the container, as a function of experimental parameters, such as type of high-explosive, container depth D, and flyer plate thickness d (cf., Fig. 1). The pressure in the olivine was then determined according to the graphical impedance match method in a pressure–particle velocity plot, using known Hugoniot data of olivine and iron (Fig. 2). The calculations show that a pressure of 56 GPa was delivered into the iron container. Assuming a single shock propagation, this corresponds to a pressure of 41 GPa in olivine. The duration of the shock compression was estimated from a time–distance diagram, which displays the propagation paths of shock, particle, and rarefaction waves (Fig. 3). This estimation reveals that the shock wave lasted ~0.7 μs in the upper part of the olivine disc in contact with the iron container. As decompression was initiated at the back of the olivine disc, the shock duration must certainly have been shorter in the lower part of the sample. Shock and post-shock temperatures were taken, or extrapolated, from the literature (Holland and Ahrens, 1997; Raikes and Ahrens, 1979) and are roughly 500 and 200 °C, respectively. Table 2 summarizes the parameters of the shock experiment.

TABLE 2. Shock parameters of high-explosive experiment on olivine.

P (GPa)	t (μs)	T_s* (°C)	T_p† (°C)
41	≤0.7	~500	~200

Abbreviations: t = shock duration; T_s = shock temperature; T_p = post-shock temperatures.
*Holland and Ahrens (1997).
†Extrapolated from Raikes and Ahrens (1979).

Transmission Electron Microscopy

The steel block with the embedded shocked olivine sample was recovered and sawn normal to the disc plane. The olivine had been pushed down the hole until it was closed by the inward-moving iron of the container (Fig. 4). A petrographic thin section was then prepared (Fig. 5). It was sufficiently large to glue several 3 mm diameter copper grids at various places onto the polished sample surface. The olivine underlying the grids was then cored out, detached from the glass slide with acetone and thinned to electron transparency by argon ion bombardment at 4.5 kV and 1 mA in a Gatan Duomill ion milling machine. Thinned samples were carbon coated and then studied with the analytical Philips CM20 FEG scanning transmission electron microscope (STEM) of the Bayerisches Geoinstitut, operating at 200 kV. Imaging and diffraction techniques employed to characterize the microstructures were weak-beam, high-resolution, and dark-field scanning techniques, as well as selected area electron diffraction.

Chemical compositions were determined with a Vantage ThermoNoran energy-dispersive x-ray (EDX) analyser, equipped with an ultra-thin Norvar window and a germanium detector. This analytical configuration enables the measurement of light elements, particularly oxygen. To quantify the compositions, we used the technique of Van Cappellen and Doukhan (1994), in which x-ray absorption is corrected on the basis of the principle of electroneutrality. This technique requires the quantification of oxygen (see also Langenhorst *et al.*, 1995). To determine the spatial distribution of elements within shock veins, concentration profiles were quantitatively measured across the veins. In particular cases,

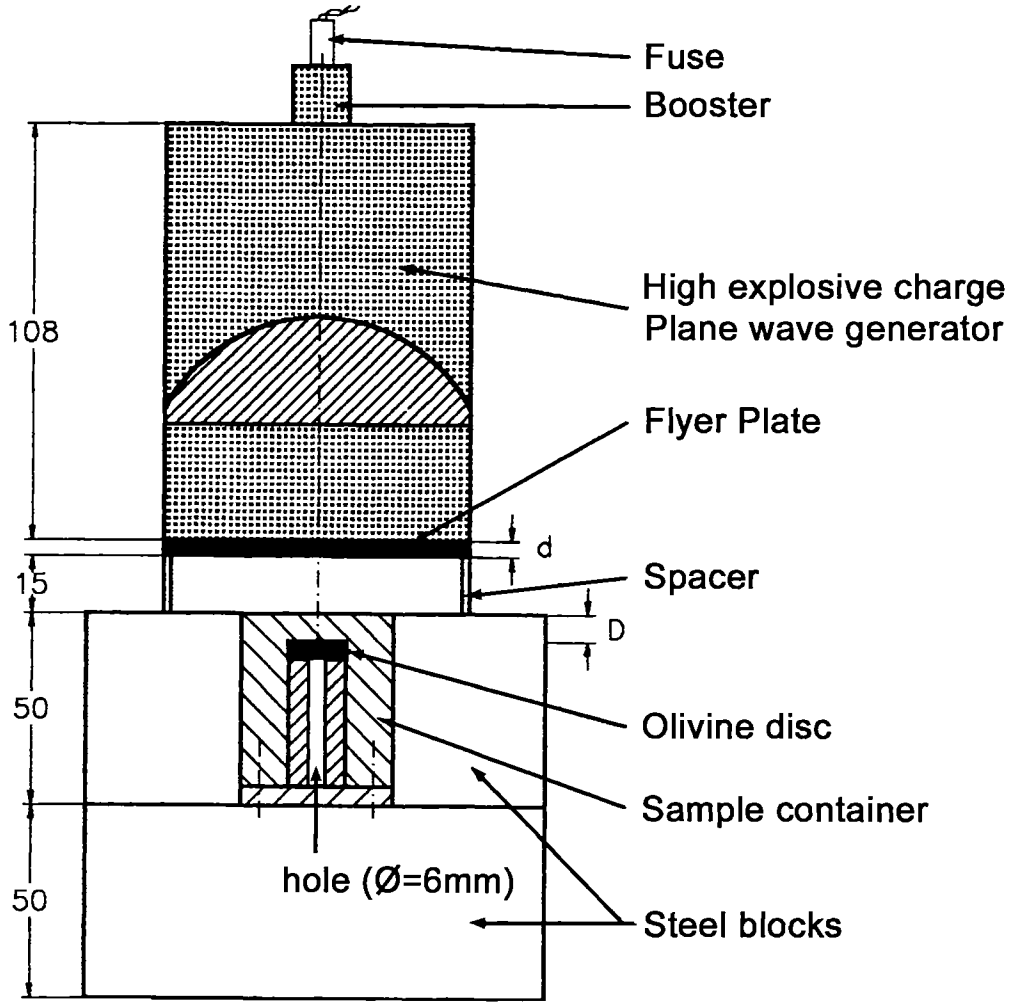

FIG. 1. Cross-section through the experimental high-explosive setup. The olivine sample is located in an iron container that has an inner cylindrical hole at the rear side of the sample.

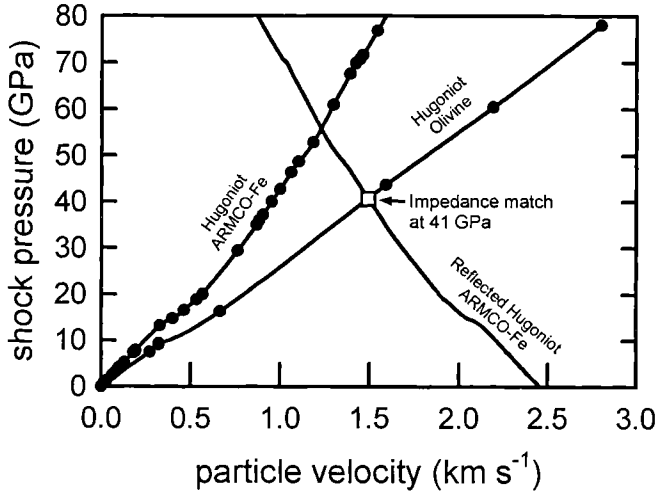

FIG. 2. Pressure–particle velocity Hugoniot diagram showing the impedance match between iron and olivine. The pressure achieved in olivine is 41 GPa.

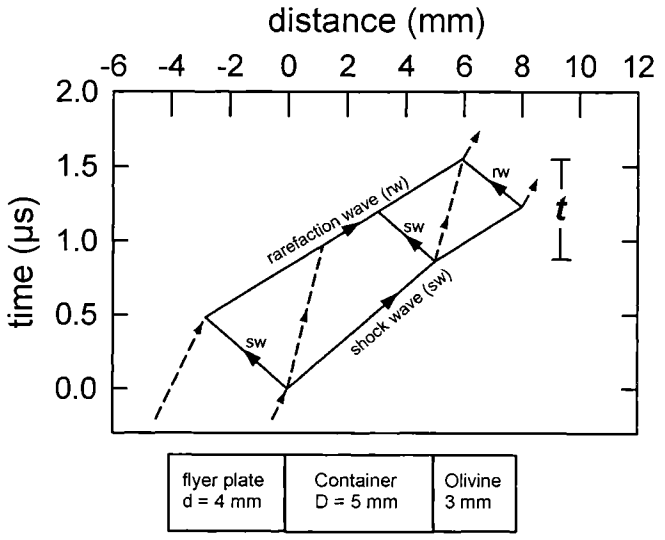

FIG. 3. Time–distance diagram showing the propagation of shock and rarefaction waves (solid lines) and the material movements (dashed lines). Based on this plot, the shock duration t in the olivine sample is estimated to be 0.7 μs.

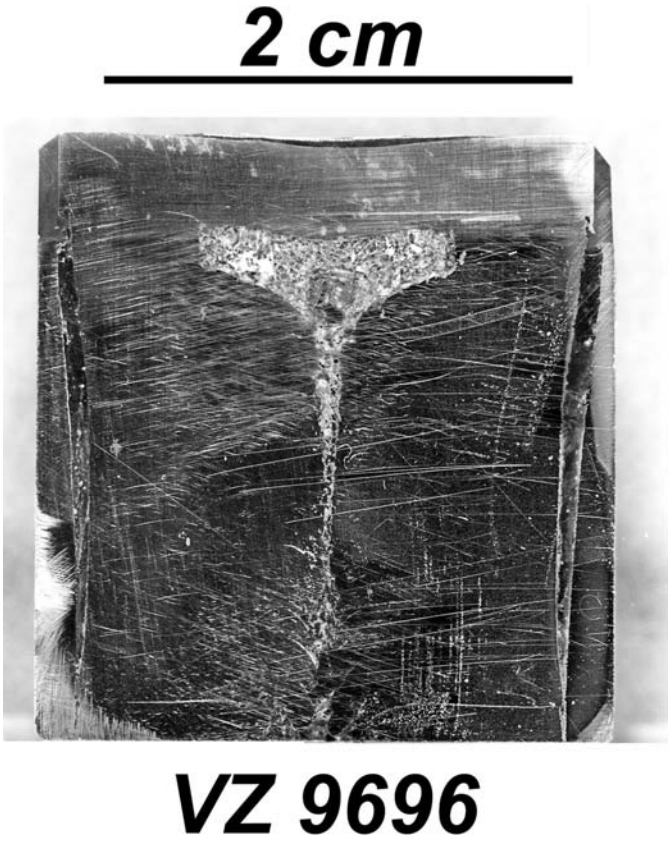

FIG. 4. Photomicrograph of a cross-section through the recovered iron container. The originally 6 mm diameter hole is completely closed by iron that flew into the empty cavity. This also led to downward flow and deformation of the olivine disc.

the distribution of elements was also mapped with the EDX-STEM combination, using a drift compensation program (see Langenhorst and Poirier, 2000a,b).

RESULTS

The macroscopic deformation of the sample resembles at a small scale the type of tectonic deformation found in graben systems at the geological scale. Thus, the deformed sample can conveniently be described in terms of tectonics, although at a much smaller scale than tectonic features in the field.

The longitudinal thin section of the sample exhibits a "graben", ~0.6 mm deep in the center (Fig. 5). Shear is localized on six to seven major "conjugate normal faults" on either side of the axis of symmetry of the graben. At higher optical magnification, it is clearly visible that the shear faults are filled with black material and sometimes contain also isolated olivine clasts. These black veins pervade the entire olivine specimen and form a fine network (Fig. 6a). They are remarkably similar to thin shock veins observed in ordinary chondrites (Fig. 6b).

At the scale of the transmission electron microscope (TEM), signs of strong deformation are observed. The originally defect-free olivine contains a high density of straight screw dislocations with Burgers vector **c** [001] (Fig. 7), typical of high strain-rate deformation (Langenhorst *et al.*, 1999) and often observed in shocked meteorites (*e.g.*, Madon and Poirier, 1983; Langenhorst *et al.*, 1995). The dislocations are emitted at the lips of rectilinear, mode II shear cracks (Fig. 7) or thin veins (Fig. 8). At the optical scale, these cracks can be identified as the so-called planar fractures (Stöffler *et al.*, 1991).

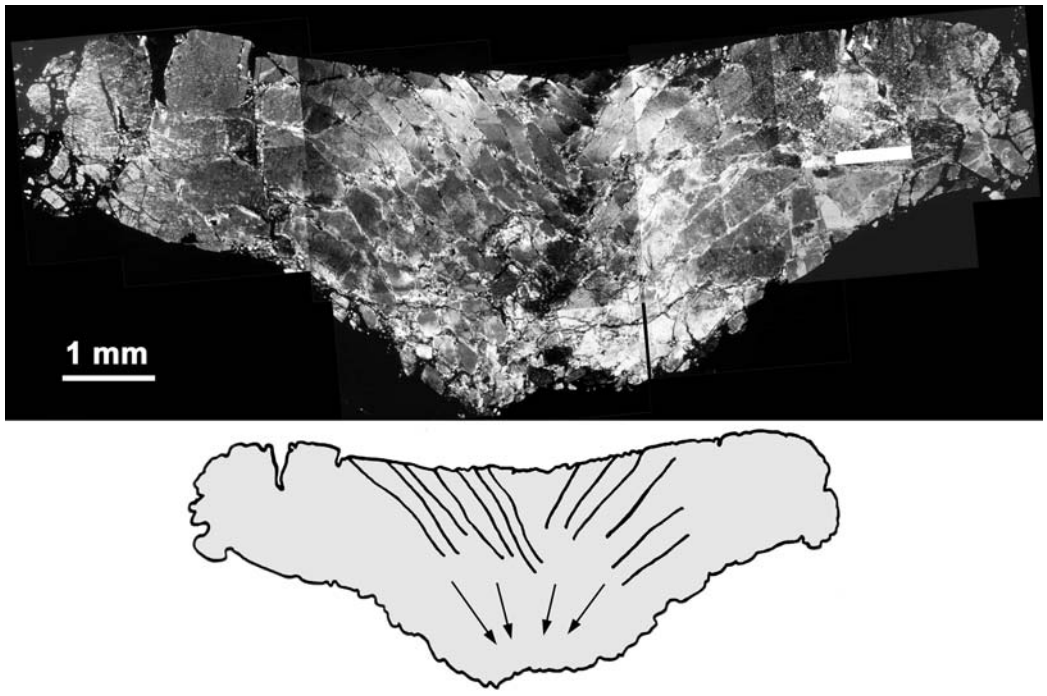

FIG. 5. Thin section of the recovered olivine sample showing a cross-section through the center of the disk between crossed nicols. The specimen has been pushed down the now closed hole and has developed numerous conjugate faults, as depicted in the sketch map.

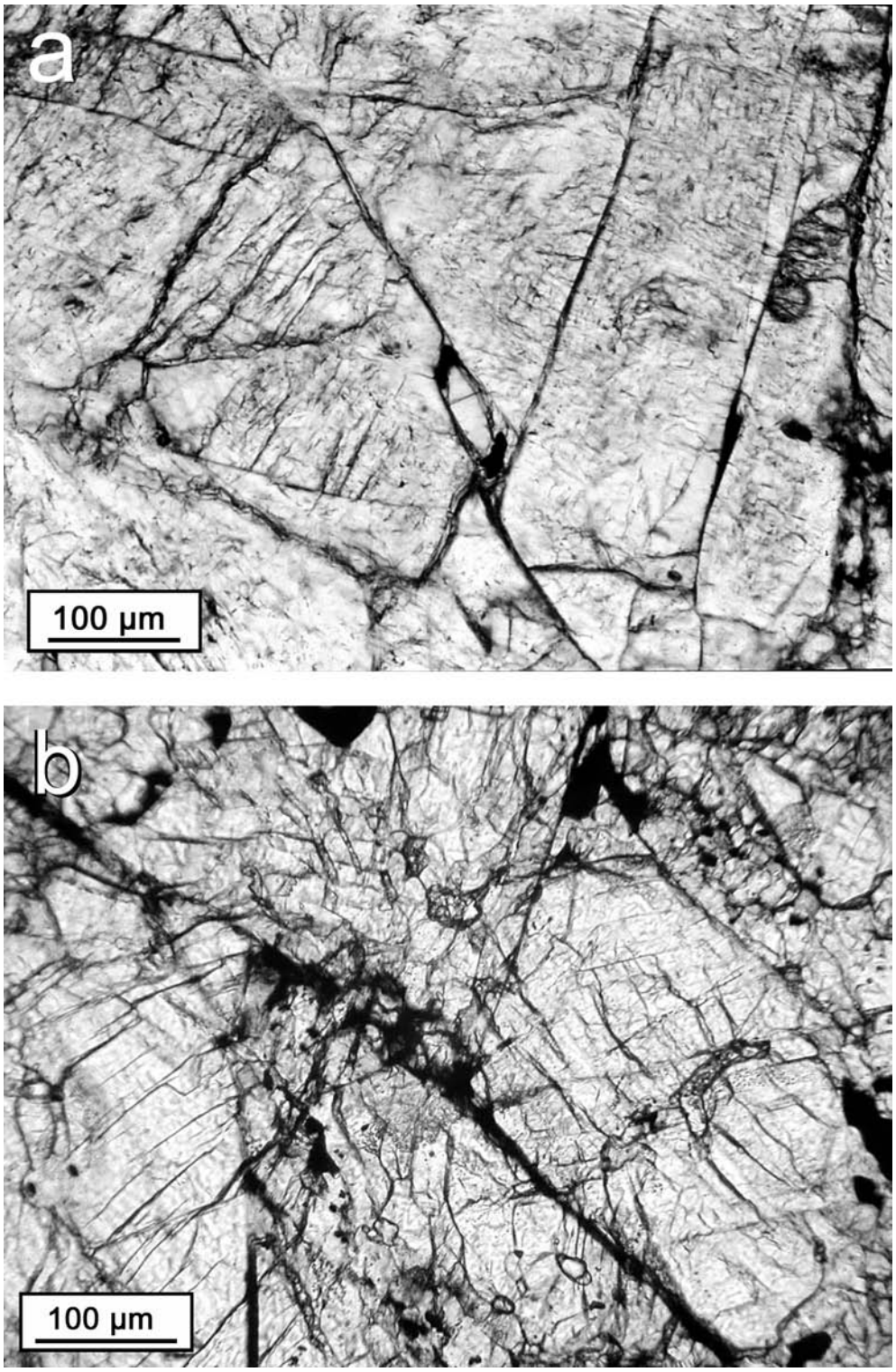

Fig. 6. Optical photomicrographs (parallel nicols) of thin shock veins in (a) the experimentally shocked single crystal olivine and (b) in an olivine-rich area in a strongly shocked L5 ordinary chondrite (Acfer 072).

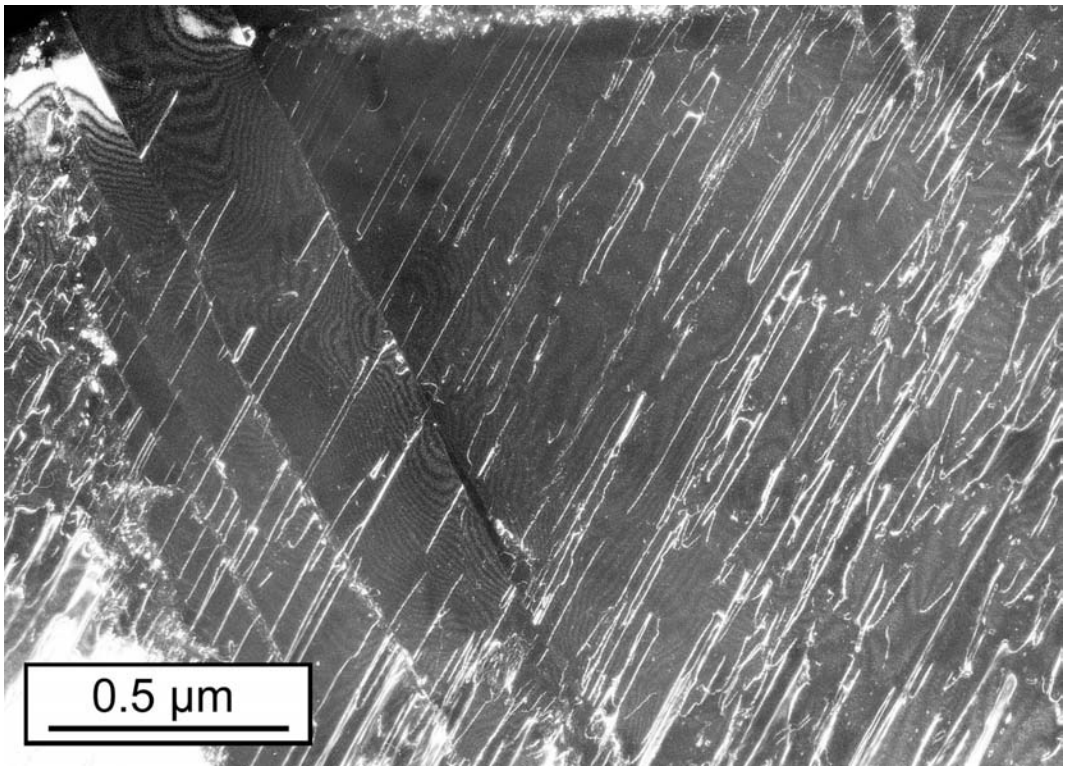

FIG. 7. Weak-beam TEM image of numerous **c** screw dislocations that have been emitted at the visible shear cracks, the so-called planar fractures.

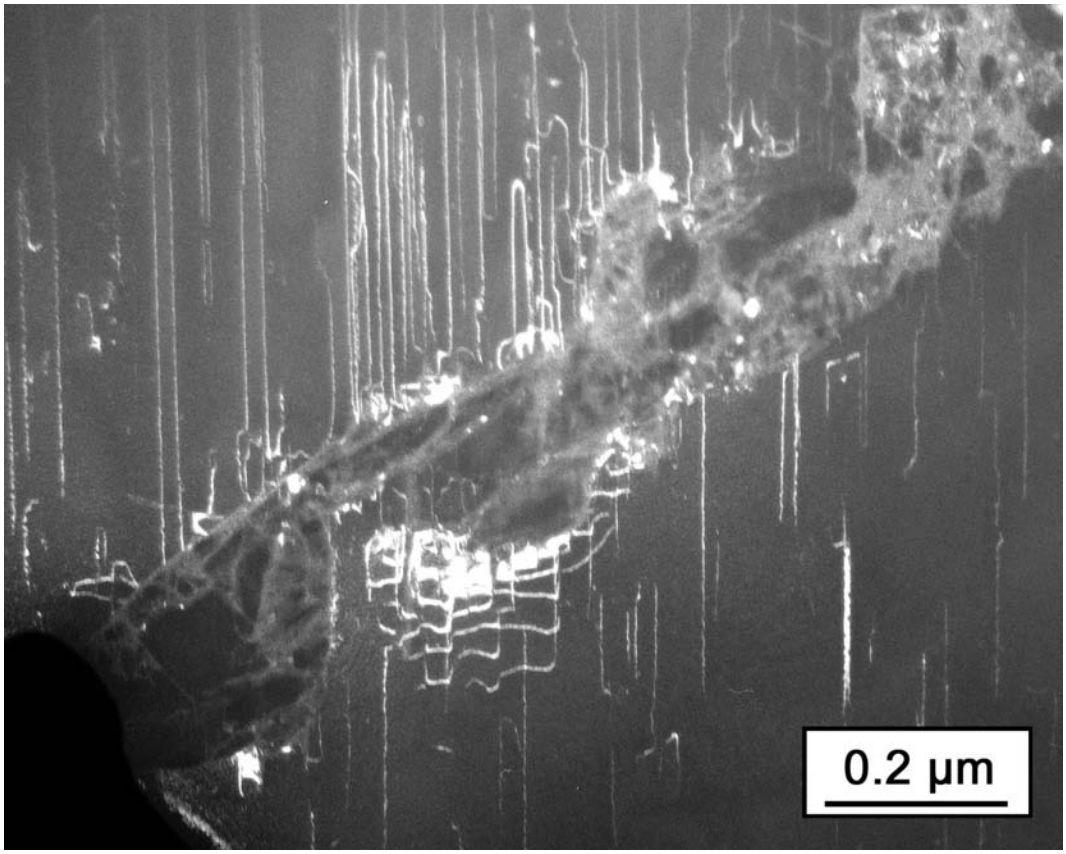

FIG. 8. Weak-beam TEM image of **c** dislocations that have been emitted at a very thin shear vein.

Thicker (up to 5–10 μm wide) veins are also observed and correspond to the macroscopic "normal faults", which resemble shock veins in chondrites. They contain small (a few hundred nanometers to half a micrometer wide) prismatic olivine crystals and scattered glass pockets (Figs. 9 and 10). Some crystals show a sub-idiomorphic tabular shape (Fig. 11a,b). The glass fills the interstitial, often triangular space between the crystals (Fig. 10). Ringwoodite and/or wadsleyite, the high-pressure polymorphs of olivine, have not been found.

The compositions of newly formed olivine crystals in one of these veins were measured along a traverse (Fig. 12a,b). They vary, quasi-periodically, between ~95 mol% forsterite, which is less iron-rich than the initial single crystal olivine, and a composition that is richer in iron, ~75 mol% forsterite (see also Table 1). As the point analyses produced visible contamination spots, their exact positions can be directly recognized in the STEM image (Fig. 12b). The comparison of the image with the measured concentration profile shows that the forsterite-rich analyses correspond to the cores of olivine crystals, whereas the rims are fayalite-rich. Additional analyses of the interstitial glass yield the iron richest compositions. These analyses can stoichiometrically be regarded as corresponding to olivine with a forsterite content as low as 29 mol% (Table 1).

DISCUSSION

Crystallization Path

The microstructure of the 10 μm thick veins points to localized melting of olivine along shear faults and subsequent crystallization of the melt during cooling. Even though cooling must have been rapid, it is not surprising that the melt did not form a glass, as it is notoriously difficult to produce glass by quenching melts of a near-forsteritic composition (cf., Jeanloz *et al.*, 1977), whereas evidence of quenched fayalite glass has been reported (Lacam *et al.*, 1980).

The quasi-periodic oscillations of compositions along the traverse reflect the zonation of crystals and are the result of fractional crystallization of the melt (Fig. 13). This crystallization probably happened after the decay of the shock wave, because most of the shearing and, hence, melting was initiated when the shock wave was reflected as a rarefaction wave at the free area at the rear surface of the sample (*i.e.*, during the rapid decompression phase). The absence of high-pressure phases also indicates crystallization near or at ambient pressure. Since the compositions of olivine cores remain the same along the vein traverse, nucleation of the crystals must have started simultaneously in the melt vein due to strong supercooling. The first nuclei had a composition more forsteritic than the initial melt and may have started to precipitate at a temperature of ~1830 °C (cf., Fig. 13). Due to rapid cooling, these nuclei could not equilibrate with the iron-enriched liquid. In the course of cooling, the crystals were, hence, overgrown by layers that successively became richer and richer in iron. The crystals finally came into mutual contact, forming a polycrystal with spatial variation of compositions. At the same time, the relic liquid also evolved to more and more iron-rich compositions until it was finally quenched as interstitial glass. The glass pockets at triple junctions between grains represent this quenched residual melt of highest iron content, with ~70 mol% fayalite component (Table 1). This composition indicates quenching and solidification at a temperature of ~1460 °C (Fig. 13).

We have recently attempted to estimate the solidification duration of shock veins by solving the so-called "Stefan" problem (Langenhorst and Poirier, 2000b; see also Turcotte and Schubert, 1982). The time for solidification depends on factors such as the thickness of the vein and the initial temperature difference between the melt vein and the adjacent bulk material. Assuming a reasonable temperature difference of ~1500 °C, we find a solidification time of ~10 μs for veins that, as in our experiment, are up to 10 μm thick. The solidification of the vein took thus 10× longer than the duration of shock. Moreover, taking into account that, due to the special geometry of our experiment, the melt veins were probably generated during the decompression phase, the shock duration of 0.7 μs was too short to allow crystallization of high-pressure minerals. In keeping with our results, high-pressure minerals have never been unambiguously observed in other shock experiments with olivine (Müller and Hornemann, 1969; Reimold and Stöffler, 1978; Bauer, 1979; Jeanloz, 1980).

In nature, however, the shock pulses are distinctly longer (up to seconds) than those in experiments due to the much larger diameter of natural projectiles (Deutsch and Langenhorst, 1998; Langenhorst *et al.*, 2002). Therefore, this kinetics problem does not apply to nature and high-pressure minerals can readily crystallize in meteorites, even if the shock veins are initiated during the late phase of decompression.

Shear Melting

As outlined above, the melt veins were probably produced during shock decompression and crystallized during cooling. As the melt veins coincide with macroscopic shear "faults", it is also reasonable to assume that shear heating caused melting. The order of magnitude calculation below supports this hypothesis.

The average "throw" of the conjugate microscopic faults is $s \approx 140\ \mu$m (Fig. 5). If we assume the width of the fault zones to be $\delta \approx 5\ \mu$m, the resultant shear is $\epsilon = s/\delta \approx 30$. The mechanical energy deposited in one fault zone, per unit volume, during the time of shearing, is $W = \sigma\epsilon$, where σ is the shear stress. The energy is mostly dissipated into heat and the temperature of the fault zone can increase locally by ΔT, with

$$\Delta T = \sigma\epsilon/\rho C_p \quad (1)$$

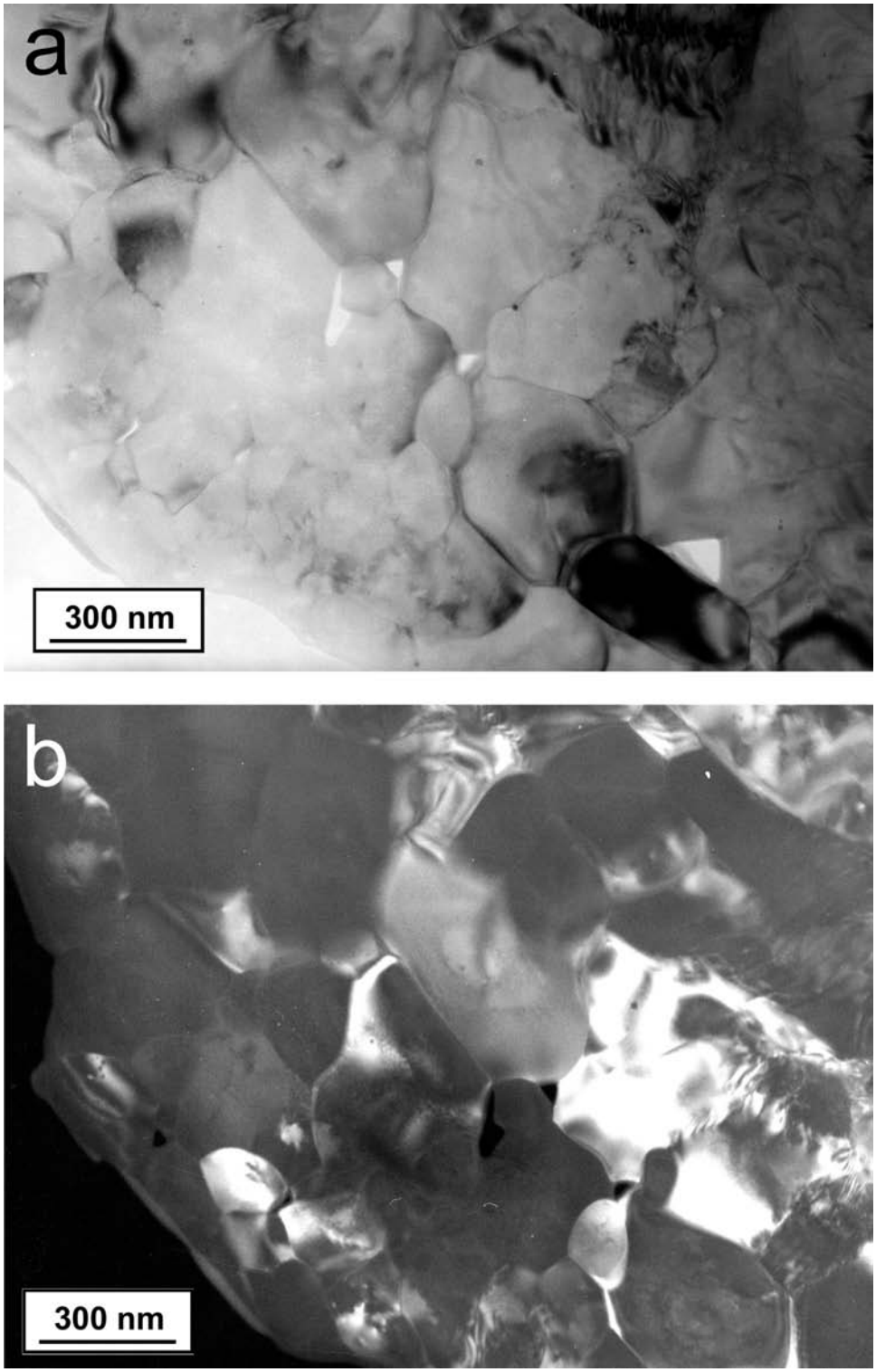

FIG. 9. Corresponding (a) bright-field and (b) dark-field TEM images of newly grown polycrystalline olivine in a shear vein.

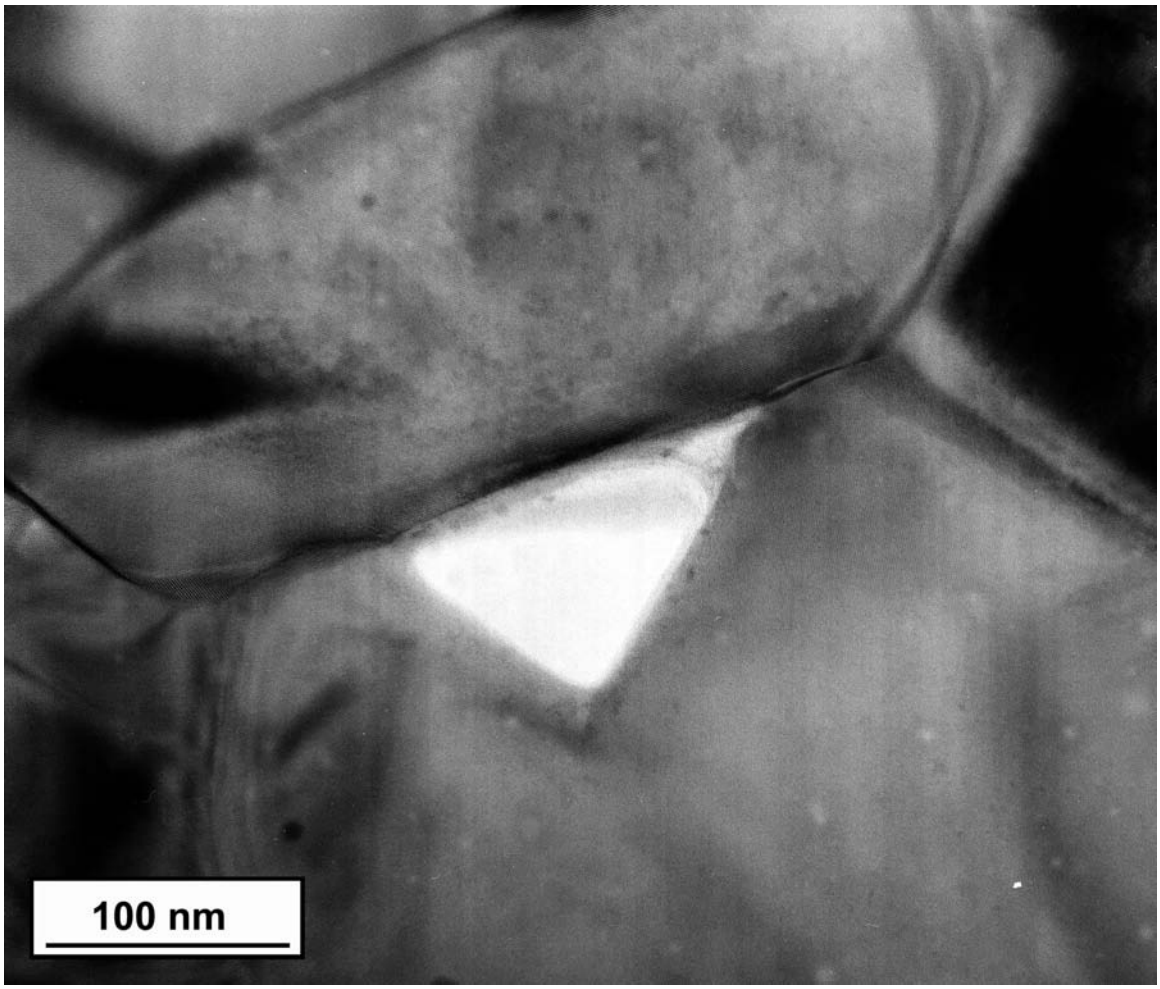

FIG. 10. Enlarged TEM view of a glass pocket between idiomorphic olivine platelets in a shear crack. Since the glass is softer than the surrounding crystals, it was preferentially thinned by ion beam bombardment and remained only in the upper part of the triangular pocket.

where ρ is the density and C_p is the specific heat per unit mass.

It is therefore possible to estimate the value of the shear stress that could lead to a temperature increase large enough to initiate melting along a shear zone. The value of the specific heat of forsterite is given in the literature as $C_p = 840$ J/kg × K (Turcotte and Schubert, 1982) or $C_p = 1330$ J/kg × K (Navrotsky, 1994). We will adopt an intermediate value: $C_p \approx 1000$ J/kg × K. Taking $\rho = 3.2 \times 10^3$ kg/m^3 for the density of olivine, the specific heat per unit volume is therefore $\rho C_p \approx 3 \times 10^6$ J/m^3 × K.

Assuming that melting would occur for $\Delta T > 3000$ K, we find, from Eq. (1), that a shear stress in excess of $\sigma \approx 3 \times 10^8$ Pa, or ~3 kbar, would be necessary to cause shear melting. This figure seems reasonable in view of the high-pressure gradients induced by the geometry of the sample used in this experiment during the shock transition. Assuming a shock duration $\tau \approx 10^{-6}$ s, this corresponds to a dissipated power $P = \sigma\epsilon/\tau \approx 10^{16}$ W/m^3. Taking the dimensions of a typical fault zone as 2.5 mm × 5 mm × 5 μm (*i.e.*, a volume of ~6×10^{-11} m^3), we may estimate that the power dissipated in one fault zone is of the order of 600 kW.

The temperature increase would mostly stay localized in the shear zone. For a shock duration $\tau \approx 10^{-6}$ s and a typical thermal diffusivity $\kappa = 10^{-6}$ m^2 s^{-1}, the penetration depth of heat into the adjacent host rock would be of the order of $(\kappa\tau)^{1/2} \approx 1$ μm (*i.e.*, much smaller than the width of a typical melt vein).

These calculations, admittedly, only provide order of magnitude estimates of the temperature increase due to shear heating. However, such as they are, they show that the veins observed in this sample are the result of shear-induced melting. The calculations also demonstrate that shock and post-shock temperatures play a negligible or even no role in the melting process, because they are one order of magnitude lower than the shear-induced temperature (Table 2). Even if there would be large shock pressure heterogeneities in the sample, for example, in our experiment a twofold increase of the pressure

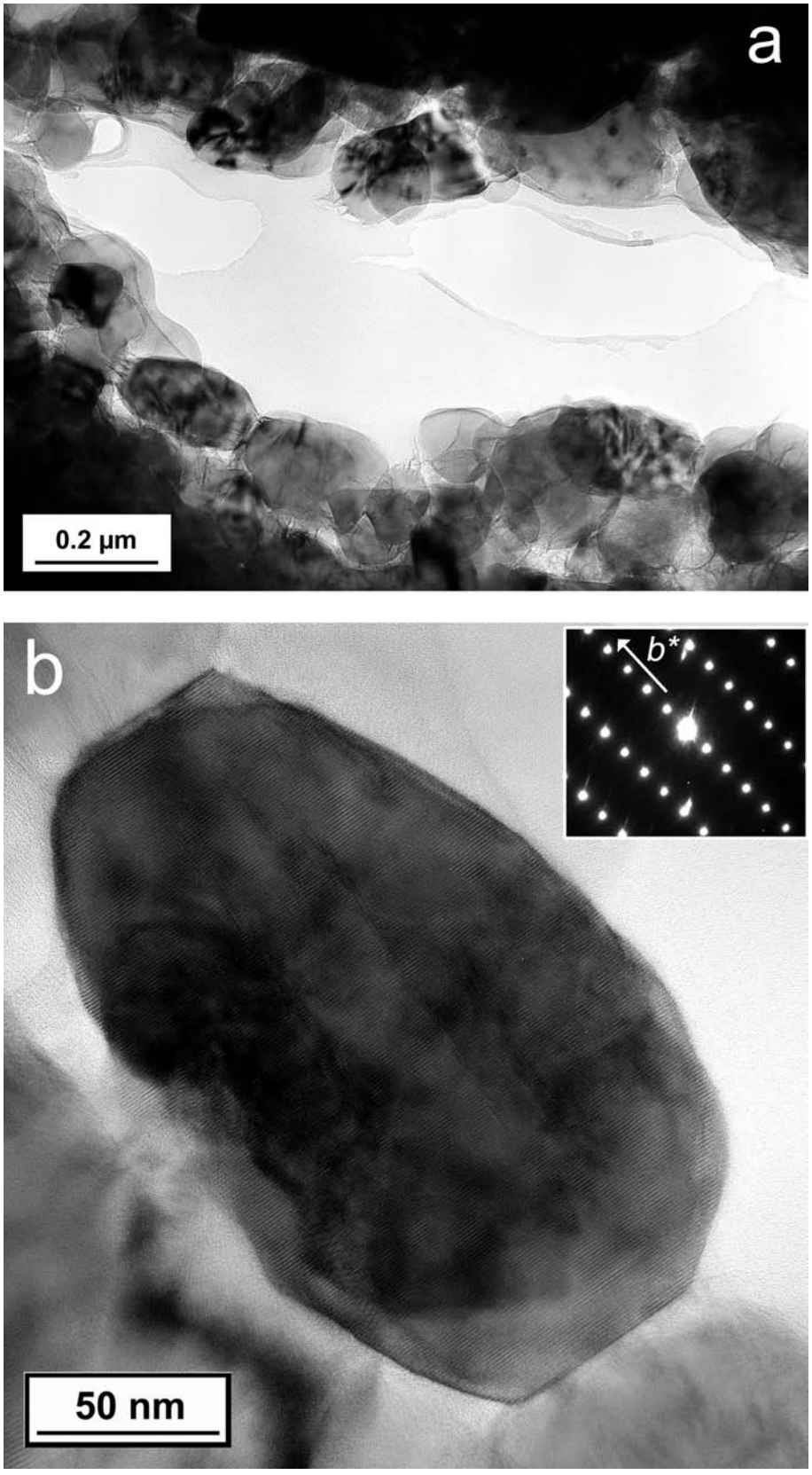

FIG. 11. (a) Bright-field TEM image of a shear crack filled with numerous olivine platelets. The enlarged view in (b) shows a high-resolution TEM image of one olivine platelet bounded in one dimension by [010] faces. The inset shows the corresponding diffraction pattern.

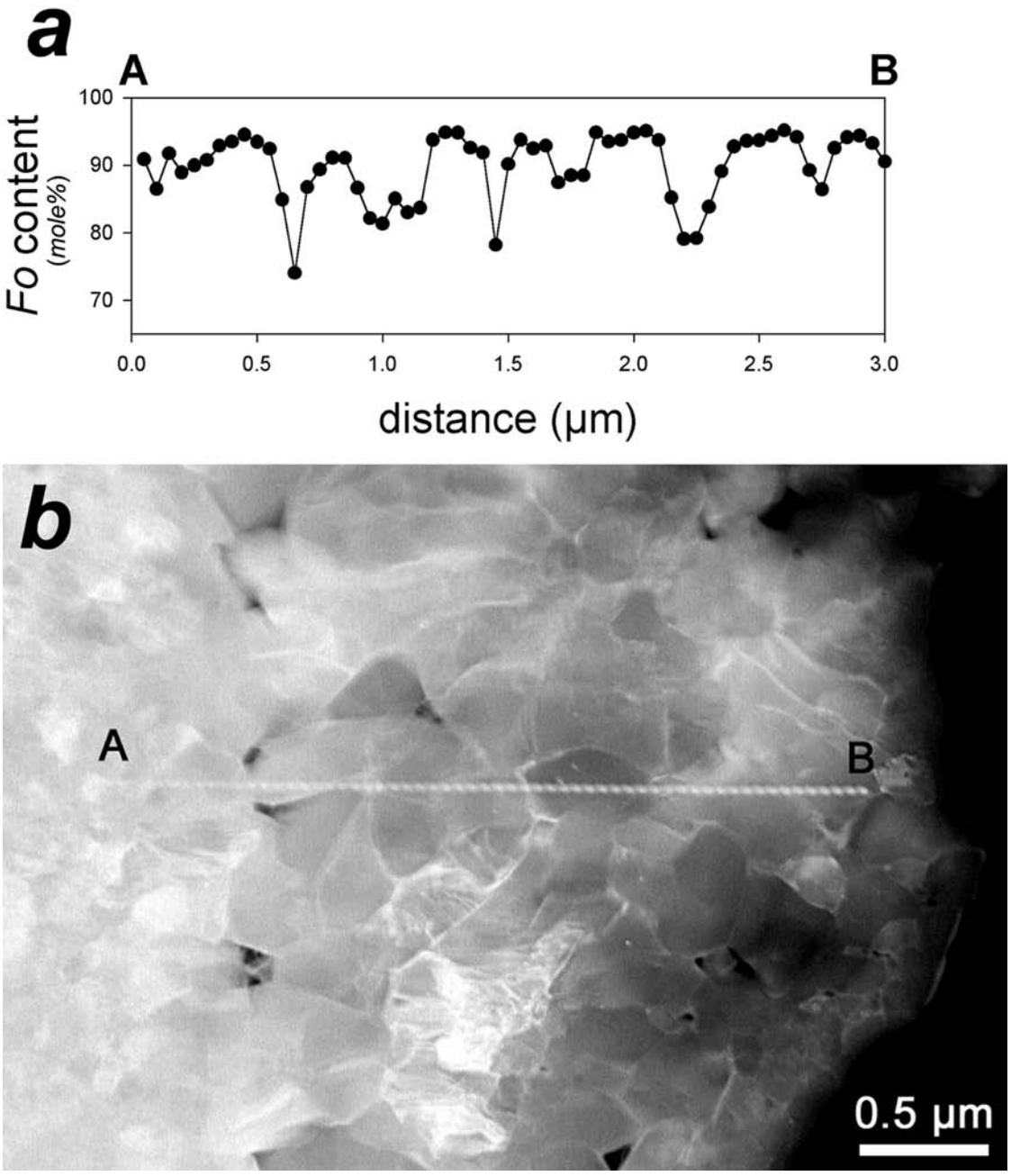

FIG. 12. (a) A 3 μm long concentration profile measured along a traverse of the shock vein. The contamination spots of analyses are visible in (b) the scanning dark-field image. The comparison of the concentration profile with the image reveals that the cores of olivine grains are enriched in Mg, whereas the rims have a distinctly higher Fe content.

(~80 GPa), measured shock temperatures (Holland and Ahrens, 1997) are still too low to melt olivine—it would stay below the solidus.

CONCLUSIONS

A single crystal olivine has been experimentally shocked in a geometry favoring significant shear. The shock experiment succeeded in reproducing the essential features observed in shocked chondrites: bulk olivine containing a high density of **c** dislocations and veins of material that was melted and then crystallized to form numerous zoned olivine crystals. The major difference is, however, the absence of high-pressure phases in our shocked sample, although they have been observed in many shocked L6 chondrites (*e.g.*, Madon and Poirier, 1983; Price *et al.*, 1983; Langenhorst *et al.*, 1995; Chen *et al.*, 1996). This difference is not surprising, if we note that the pressure duration in the shock-wave experiment (~1 μs) is

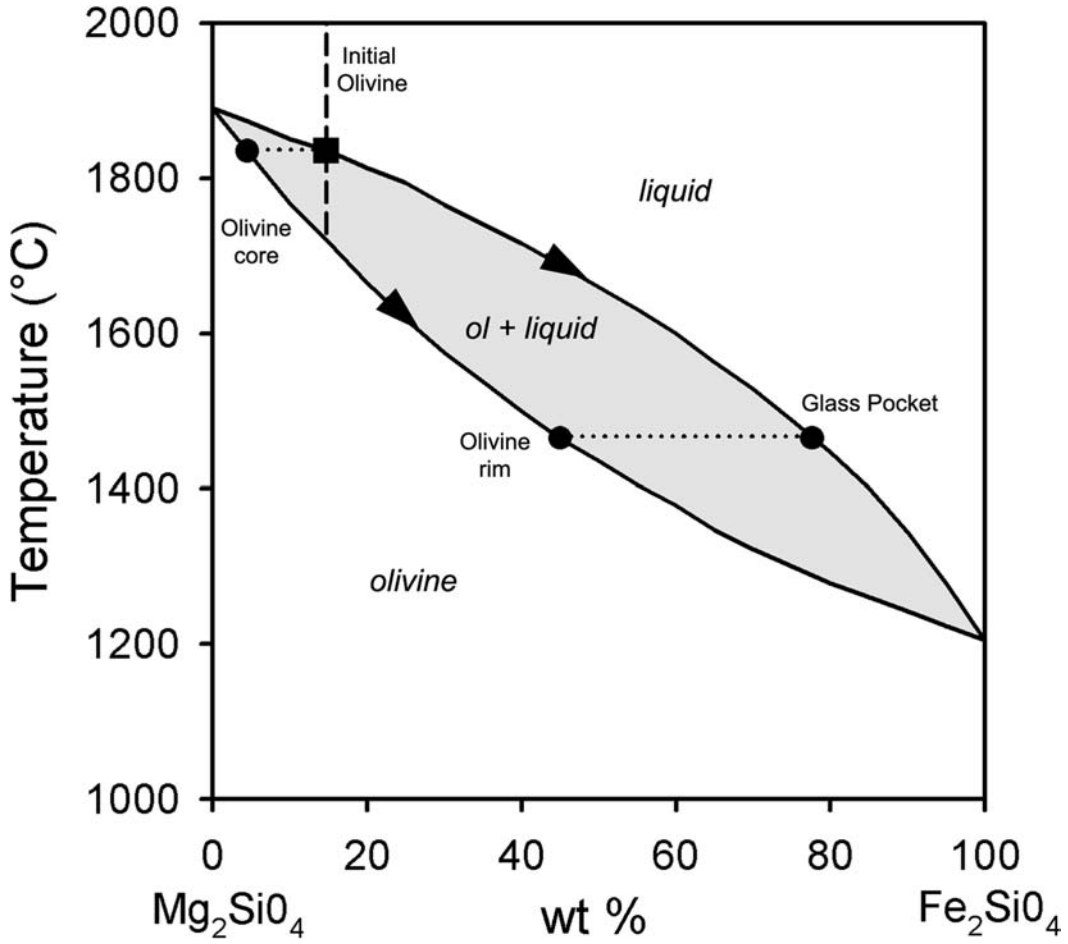

FIG. 13. The olivine phase diagram by Bowen and Schairer (1935) (in wt%) displaying schematically the fractional crystallization path observed in a shock vein. Data points on the liquidus are given in wt% Mg_2SiO_4 and represent analyses in Table 1, whereas points on the solidus are the expected, most extreme compositions for rim and core regions of olivine. Under equilibrium conditions the crystallization would have ended at ~1700 °C with homogeneous olivine crystals of a composition identical to that of the initial olivine (square). Due to fast quenching and fractional crystallization we observed large compositional heterogeneity with forsterite-rich olivine cores as well as fayalite-rich olivine rims and glass pockets (dots).

~6 orders of magnitude shorter than in the case of shocked meteorites (~1 s; see, for example, Deutsch and Langenhorst, 1998). Therefore, the experimentally produced melt veins started crystallizing when the shock wave had already decayed.

The small idiomorphic olivine grains with large compositional variations and the residual glass pockets enriched in iron point to fractional crystallization of the melt along the faults. An order of magnitude calculation shows that temperatures high enough to cause melting may have been reached by shear heating, assuming values of shear stresses compatible with the shock experiment. This experiment substantiates that shock veins in meteorites are caused by shear heating rather than by pressure heterogeneities.

Acknowledgments–We are indebted to S. Mackwell (BGI), who provided the large gem-quality olivine crystal. We are also grateful to F. Bartschat (IfP) and J. Hopf (BGI) for preparing figures and to U. Heitmann (IfP), R. Thewes (IfP), B. Nasdala (EMI), and D. Franz (EMI) for technical support. One of us (J. P. P.) thanks the Alexander von Humboldt Stiftung for a Research Award, which made this collaboration possible, and the Bayerisches Geoinstitut for its hospitality. This study was supported by the DFG (DE 401/15, HO 1446/3 and LA 830/4) and the Fonds der Chemischen Industrie (grant to F. Seifert). We thank W. U. Reimold and J. G. Spray for constructive reviews.

Editorial handling: R. A. F. Grieve

REFERENCES

BOWEN N. L. AND SCHAIRER J. F. (1935) The system MgO–FeO–SiO_2. *Am. J. Sci.* **29**, 151–217.

BAUER J. F. (1979) Experimental shock metamorphism of mono- and polycrystalline olivine. *Proc. Lunar Sci. Conf.* **10th**, 2573–2596.

CHEN M., SHARP T. G., EL GORESY A., WOPENKA B. AND XIE X. (1996) The majorite-pyrope + magnesiowüstite assemblage: Constraints on the history of shock veins in chondrites. *Science* **271**, 1570–1573.

DEUTSCH A. AND LANGENHORST F. (1998) Mineralogy of astroblems. In *Advanced Mineralogy*, vol. 3 (ed. A. S. Marfunin), pp.76–95. Springer, Berlin, Germany.

HORNEMANN U. AND MÜLLER W. F. (1971) Shock-induced deformation twins in clinopyroxene. *Neues Jahrb. Mineral. Mh.* **6**, 247–256.

HOLLAND K. G. AND AHRENS T. J. (1997) Melting of $(Mg,Fe)_2SiO_4$ at the core–mantle boundary of the Earth. *Science* **275**, 1623–1625.

IVANOV B. A., LANGENHORST F., DEUTSCH A. AND HORNEMANN U. (2002) How strong was impact-induced CO_2 degassing in the K/T event? Numerical modeling of laboratory experiments. In *Catastrophic Events and Mass Extinctions: Impacts and Beyond* (eds. C. Koeberl and K. G. MacLeod), pp. 587–594. Geol. Soc. Am. Spec. Paper **356**, Boulder, Colorado, USA.

JEANLOZ R. (1980) Shock effects in olivine and implications for Hugoniot data. *J. Geophys. Res.* **85**, 3163–3176.

JEANLOZ R., AHRENS T. J., LALLY J. S., NORD G. L., CHRISTIE J. M. AND HEUER A. H. (1977) Shock-produced olivine glass: First observations. *Science* **197**, 457–459.

KENKMANN T., HORNEMANN U. AND STÖFFLER D. (2000) Experimental generation of shock-induced pseudotachylites along lithological interfaces. *Meteorit. Planet. Sci.* **35**, 1275–1290.

LACAM A., MADON M. AND POIRIER J. P. (1980) Olivine glass and spinel formed in a laser heated, diamond-anvil high pressure cell. *Nature* **289**, 155–157.

LANGENHORST F. AND DEUTSCH A. (1994) Shock experiments on pre-heated α- and β-quartz: I. Optical and density data. *Earth Planet. Sci. Lett.* **125**, 407–420.

LANGENHORST F. AND POIRIER J. P. (2000a) "Eclogitic" minerals in a shocked basaltic meteorite. *Earth Planet. Sci. Lett.* **176**, 259–265.

LANGENHORST F. AND POIRIER J. P. (2000b) Anatomy of black veins in Zagami: Clues to the formation of high-pressure phases. *Earth Planet. Sci. Lett.* **184**, 37–55.

LANGENHORST F., JOREAU P. AND DOUKHAN J. C. (1995) Thermal and shock metamorphism of the Tenham chondrite: A TEM examination. *Geochim. Cosmochim. Acta* **59**, 1835–1845.

LANGENHORST F., BOUSTIE M., MIGAULT A. AND ROMAIN J. P. (1999) Laser shock experiments with nanoseconds pulses: A new tool for the reproduction of shock defects in olivine. *Earth Planet. Sci. Lett.* **173**, 333–342.

LANGENHORST F., BOUSTIE M., DEUTSCH A., HORNEMANN U., MATIGNON CH., MIGAULT A. AND ROMAIN J. P. (2002) Experimental techniques for the simulation of shock metamorphism: A case study on calcite. In *High-pressure Shock Compression of Solids—Shock Chemistry with Applications to Meteorite Impacts* (eds. L. Davison, Y. Horie and T. Sekine), pp. 1–27. Springer, New York, New York, USA.

MADON M. AND POIRIER J. P. (1983) Transmission electron microscope observation of microscope observation of α, β and γ $(Mg,Fe)_2SiO_4$ in shocked meteorites: Planar defects and polymorphic transitions. *Phys. Earth Planet. Interiors* **33**, 31–44.

MÜLLER W. F. AND HORNEMANN U. (1969) Shock-induced planar deformation structures in experimentally shock-loaded olivines and in olivines from chondritic meteorites. *Earth Planet. Sci. Lett.* **7**, 251–264.

NAVROTSKY A. (1994) *Physics and Chemistry of Earth Materials.* Cambridge Univ. Press, New York, New York, USA. 417 pp.

PRICE G. D., PUTNIS A., AGRELL S. O. AND SMITH D. G. W. (1983) Wadsleyite, natural β-$(Mg,Fe)_2SiO_4$ from the Peace River meteorite. *Can. Mineral.* **21**, 29–35.

RAIKES S. A. AND AHRENS T. J. (1979) Post-shock temperatures in minerals. *Geophys. J. Royal Astron. Soc.* **58**, 717–747.

REIMOLD W. U. AND STÖFFLER D. (1978) Experimental shock metamorphism of dunite. *Proc. Lunar Planet. Sci. Conf.* **9th**, 2805–2824.

SPRAY J. G. (1987) Artificial generation of pseudotachylite using friction welding apparatus: Simulation of melting on a fault zone. *J. Struct. Geol.* **9**, 49–60.

STÖFFLER D., BISCHOFF A., BUCHWALD V. AND RUBIN A. E. (1988) Shock effects in meteorites. In *Meteorites and the Early Solar System* (eds. J. F. Kerridge and M. S. Matthews), pp. 165–202. Univ. Arizona Press, Tucson, Arizona, USA.

STÖFFLER D., KEIL K. AND SCOTT E. R. D. (1991) Shock metamorphism of ordinary chondrites. *Geochim. Cosmochim. Acta* **55**, 3845–3867.

TURCOTTE D. L. AND SCHUBERT G. (1982) *Geodynamics: Applications of Continuum Physics to Geological Problems.* John Wiley & Sons, New York, New York, USA. 450 pp.

VAN CAPPELLEN E. AND DOUKHAN J. C. (1994) Quantitative x-ray microanalysis of ionic compounds. *Ultramicroscopy* **53**, 343–349.

VAN DER BOGERT C. H., SCHULTZ P. H. AND SPRAY J. G. (2000) Defining the petrology of pseudotachylytes in ordinary chondrites: An experimental and deductive approach (abstract). *Lunar Planet. Sci.* **31**, #1962, Lunar and Planetary Institute, Houston, Texas, USA (CD-ROM).